Crystal Structure Determination of α, β and γ-Bi4V2O11 Polymorphs. Part 1. γ and β-Bi4V2O11

ARTICLE *in* SOLID STATE SCIENCES · JUNE 2003

Impact Factor: 1.84 · DOI: 10.1016/S1293-2558(03)00015-3

6 AUTHORS, INCLUDING:

Pascal Roussel
National Graduate School of Engineering C…
314 PUBLICATIONS **2,090** CITATIONS
SEE PROFILE

Rose-Noelle Vannier
Université des Sciences et Technologies de …
121 PUBLICATIONS **1,808** CITATIONS
SEE PROFILE

Caroline Pirovano
National Graduate School of Engineering C…
50 PUBLICATIONS **485** CITATIONS
SEE PROFILE

Available online at www.sciencedirect.com
SCIENCE DIRECT®
Solid State Sciences 5 (2003) 851–859
Solid State Sciences
www.elsevier.com/locate/ssscie

Crystal structure determination of α, β and γ-$Bi_4V_2O_{11}$ polymorphs. Part I: γ and β-$Bi_4V_2O_{11}$

G. Mairesse [a,*], P. Roussel [a], R.N. Vannier [a], M. Anne [b], C. Pirovano [a], G. Nowogrocki [a]

[a] *Laboratoire de cristallochimie et physicochimie du solide, UMR-CNRS 8012, ENSCL, Université des sciences et technologies de Lille, B.P. 108, 59652 Villeneuve d'Ascq cedex, France*

[b] *Laboratoire de cristallographie CNRS, UPR-CNRS 5031, B.P. 166, 38042 Grenoble cedex 09, France*

Received 25 September 2002; accepted 22 October 2002

Abstract

Using combined X-ray single crystal and neutron powder thermodiffraction data, the crystal structure of the high temperature γ-form of $Bi_4V_2O_{11}$ was confirmed and accurately refined in the *I*4/*mmm* space group and that of the β-form was entirely determined in the centrosymmetric *Amam* space group. The two-fold superlattice characterising the β structure is the result of an ordering process involving corner-sharing V–O tetrahedra and disordered trigonal bipyramids. A possible scheme for the $\gamma \leftrightarrow \beta$ phase transition is proposed.

Keywords: Oxide ion conductor; Crystal structure; Neutron diffraction; Bismuth-based materials; $Bi_4V_2O_{11}$

1. Introduction

$Bi_4V_2O_{11}$ is a rather recent compound evidenced in the late eighties, and especially studied for two classes of physical properties: (i) at room temperature it is a dielectric (ferroelectric and pyroelectric) material [1–9] and (ii) it is the parent compound of the BIMEVOX family of materials exhibiting attractive oxide anion conduction at moderate temperature [10–21].

Despite the numerous papers devoted to this compound, the knowledge of the crystal structure of the $Bi_4V_2O_{11}$ polymorphs remains very limited up to now. $Bi_4V_2O_{11}$ belongs to the Aurivillius structural type, with general formula $(Bi_2O_2)(A_{m-1}B_mO_{3m+1})$, consisting of an intergrowth between $(Bi_2O_2)^{2+}$ sheets and $(A_{m-1}B_mO_{3m+1})^{2-}$ perovskite-like layers with m the number of BO_6 octahedra stacked along the direction perpendicular to the sheets. When $m = 1$, the typical stoichiometric members are Bi_2WO_6 and δ-Bi_2MoO_6, where the perovskite layer is reduced to a single ReO_3-type slab. $Bi_4V_2O_{11}$ or $Bi_2VO_{5.5}$ is the corresponding intrinsic oxygen deficient compound $(Bi_2O_2)(VO_{3.5}\square_{0.5})$ and exhibits, versus temperature, three main polymorphs α monoclinic, β orthorhombic and γ tetragonal. They can all be described from a mean orthorhombic subcell $a_m \approx 5.53$, $b_m \approx 5.61$ and $c_m \approx 15.29$ Å (stacking direction). The relationships between the polymorph unit cell parameters are: $a_\gamma = b_\gamma = a_m/\sqrt{2}$, $c_\gamma = c_m$; $a_\beta = 2a_m$, $b_\beta = b_m$, $c_\beta = c_m$; $a_\alpha = 6a_m$, $b_\alpha = b_m$ and $c_\alpha = c_m$. The small monoclinic distortion occurring in the α-polymorph [22,23] disappears rapidly with a small amount of impurity, likely substituting for vanadium. The parameter evolution versus temperature has already been reported [22, 24] and moreover, the ferroelastic character of the $\alpha \leftrightarrow \beta$ phase transition has been evidenced using single crystal X-ray thermodiffraction [24].

The crystal structure of the high temperature γ-polymorph was already described in the *I*4/*mmm* space group from single crystal X-ray diffraction data collected at 550 °C [11]. For the β-polymorph, only a partial determination was reported from single crystal X-ray diffraction data collected at 440 °C using the *Amam* orthorhombic space group, but the O atoms of the vanadium surrounding could not be located at this time [25]. There are very large discrepancies between the α-$Bi_4V_2O_{11}$ structures presented in different papers and moreover the descriptions are often limited to that of the orthorhombic subcell [22,26–29].

The knowledge of the real crystal structures is a prerequisite to understand the $\alpha \leftrightarrow \beta$ and $\beta \leftrightarrow \gamma$ reversible phase transitions observed by diffraction methods (X-ray, neutron

* Corresponding author.
E-mail address: mairesse@ensc-lille.fr (G. Mairesse).

1293-2558/03/$ – see front matter
doi:10.1016/S1293-2558(03)00015-3

and electron), thermal analysis and impedance spectroscopy, and to correlate the macroscopic properties of $Bi_4V_2O_{11}$ with the structural parameters at the atomic level. At this aim, X-ray single crystal and neutron powder diffraction data were used in combined refinements. The γ and β forms are the topic of this first paper. A second paper will be devoted to the α polymorph.

2. Experimental

Synthesis of powdered $Bi_4V_2O_{11}$ was performed by classical solid state reaction from stoichiometric amounts of reagent grade pure oxides: Bi_2O_3 (Riedel de Hahn 99.5%) decarbonated at 600 °C and V_2O_5 (Aldrich 99.6%). The oxides were thoroughly ground in an agate mortar and fired in Au foil boats at 600 °C, 700 °C and finally 800 °C for 12 h with intermediate regrindings. As the oxygen stoichiometry in $Bi_4V_2O_{11}$ is a critical point and is strongly depending on the preparation conditions [23,29], to obtain a fully oxidised compound, the prepared material was slowly cooled in air from the last firing temperature to 300 °C at a 5 °C/h rate and then to room temperature at a 10 °C/h rate. To check this problem of oxygen stoichiometry, a thermogravimetric analysis was performed on a Setaram TGA 92.

$Bi_4V_2O_{11}$ is the upper limit of a small solid solution domain within the Bi_2O_3–V_2O_5 binary diagram, extending towards the Bi-rich compositions, due to the ability of some Bi^{3+} cations to substitute for vanadium ones: $Bi_2V_{1-x}Bi_xO_\delta$ [23,30]. Starting the synthesis with a stoichiometric 2 Bi/V ratio, some Bi^{3+} substitute for V sites according to the above formula, producing some $BiVO_4$ impurity.

The purity of the resulting samples was checked by X-ray diffraction using a Guinier–De Wolff focusing camera (Cu $K\alpha$ radiation) and a Siemens D 5000 goniometer (Cu $K\alpha$ radiation) equipped with a secondary graphite monochromator. A monoclinic α-polymorph was obtained together with a small amount of $BiVO_4$ impurity, as expected. This impurity was taken into account for the following neutron powder refinements.

Neutron powder diffraction data were collected on the D1A diffractometer at the Institut Laue Langevin (ILL). Approximately 20 g of sample were introduced in a 12 mm diameter silica tube and data were collected in the range $0 \leqslant 2\theta \leqslant 154.45°$ with a step of 0.05° and a wavelength of $\lambda = 1.9089$ Å for 9 and 10 hours, at 500 °C and 670 °C, respectively. Data in the range $10 \leqslant 2\theta \leqslant 150°$ were selected for the refinements.

Single crystals were grown using a flux method. According to the Bi_2O_3–V_2O_5 phase diagram [31,32], the desired phase is close to congruent melting and its primary field of crystallisation is quite small and located on the vanadium-rich side of the normal composition. Consequently, the crystallisation of $Bi_4V_2O_{11}$ was performed from slightly V_2O_5 rich melts, the V_2O_5 excess acting as a flux. The best crystals were grown using the following conditions: gold crucible (25 ml) in air, starting composition 36 mol% V_2O_5, muffle furnace with maximum soaking temperature 900 °C, cooling to 865 °C at 1 °C/h (partial melting peritectic temperature $T_m \approx 875$ °C) and then thermal cycling similar to that used for the powder. The chemical composition was controlled by EDX analysis and was in accordance with the expected formulation within the experimental uncertainty.

Platelet-shaped crystals with large, well-developed (001) planes were obtained. The quality of these single crystals was carefully checked using polarised light of an optical microscope. Several crystals were selected and tested using X-ray diffraction. Only very thin crystals (thickness $\approx$ 10 μm) were revealed to be untwinned, single domain, with a monoclinic unitcell and superlattice peaks along the crystallographic *a* axis.

For high temperature study of the β and γ-polymorphs, the single crystal sample was cautiously wedged into the walls of a narrowed quartz capillary. Actually, two different single crystals were used for the whole study of the three phases, the first one selected for the α-form crystal structure determination being damaged when we attempted to introduce it into the capillary for the high temperature characterization.

A Phillips PW 1100 diffractometer equipped with an air blowing heating device (A.E.T. Grenoble) was used. Two sets of data were collected, one at 500 °C and the other at 670 °C.

Unit cell parameters, experimental conditions and accuracy factors for neutron and X-ray data collections are reported in Table 1. Sirpow [33] and Fullprof [34] softwares were used for the structure determinations.

3. Results and discussion

3.1. Oxygen stoichiometry of $Bi_4V_2O_{11}$

A TGA of the $Bi_4V_2O_{11}$ powder was carried out under air to control the stoichiometry of this compound versus temperature. Prior to this TGA the powder was annealed under pure oxygen for 12 h at 800 °C and slowly cooled (20 °C/h) in the same atmosphere. The corresponding heating and cooling TGA curves in air are shown in Fig. 1. The loss and gain in weight, due to some $V^V \leftrightarrow V^{IV}$ transformation, are clearly reversible under the experimental conditions. The onset temperature of the oxygen loss is about 550 °C and under isothermal conditions at 800 °C for 24 h, no deviation is observed. The deduced O content at 800 °C is 10.984 provided the starting one was exactly 11. This value is in agreement with that of 10.98 obtained from similar experiment [22]. At 670 °C, temperature of the data collection for the γ-polymorph, the O content is close to 10.99 and at 500 °C, for the β-form, the stoichiometry is 11. Thereby we considered that the O content to take into account for both γ- and β-forms was 11, within the experimental uncertainty.

Table 1
Data collection and structure refinement for γ and β $Bi_4V_2O_{11}$

	γ-$Bi_4V_2O_{11}$		β-$Bi_4V_2O_{11}$
Space group	*I*4/*mmm* (No. 139)		*Amam* (No. 63)
Unit cell parameters			
a (Å)	3.99176(4)		11.2333(2)
b (Å)	3.99176(4)		5.64925(7)
c (Å)	15.4309(3)		15.3471(2)
Unit cell volume (Å^3)	245.878(5)		973.92(3)
Z	1		4
Formula mass (g mol^{-1})		1113.80	
ρ (g cm^{-3})	7.525		7.599
Neutron powder data (ILL, D1A)			
Radiation		1.9089 Å	
2θ range, step (°), time (h),	10–150, 0.05, 10		10–150, 0.05, 9
Temperature (°C)	670		500
No. of reflections for $Bi_4V_2O_{11}$ pattern	65		316
No. of reflections for $BiVO_4$ pattern (impurity)	93		93
X-ray single crystal data (Philips PW1100)			
X-ray radiation		Mo $K\alpha$ ($\lambda = 0.71073$ Å)	
μ (Mo $K\alpha$) (cm^{-1})		702	
2θ range (°)		5–60°	
Limiting faces and distances	0 0 1		0.0004 cm
from an arbitrary origin	0 0 −1	0.0004 cm	
	6 1 0	0.0133 cm	
	−6 1 0	0.0115 cm	(indexed in the β unit cell)
	−2 1 1 0	0.0080 cm	
	0 −1 0	0.0142 cm	
	6 −1 0	0.0131 cm	
	1 0 0	0.0110 cm	
Limiting indices	$-3 \leqslant h \leqslant 5$, $-5 \leqslant k \leqslant 3$, $0 \leqslant l \leqslant 18$		$-13 \leqslant h \leqslant 13$, $-6 \leqslant k \leqslant 6$, $0 \leqslant l \leqslant 18$
No. of reflection collected	299		1675
No. of independent reflections	99 with $I > 3\sigma(I)$		322 with $I > 3\sigma(I)$
Transmission factor range		0.011–0.101	
R_{int} (after absorption correction)	4.0%		4.3%
Refinement method		Full matrix least square on F^2 (Fullprof) [34]	
Total No. of refined parameters	90		114
No. of global refined parameters	58 (incl. 57 points of background)		42 (incl. 41 points of background)
No. of profile refined parameters	14		15
No. of intensity-dependent refined parameters	17		57
Final reliability factors			
Profile	$R_p = 2.8\%$, $R_{wp} = 4.2\%$, $R_E = 1.9\%$		$R_p = 3.1\%$, $R_{wp} = 4.6\%$, $R_E = 1.9\%$
X-ray data	$R_{F^2} = 9.6\%$, $R_{F^2w} = 12.3\%$, $R_F = 5.5\%$		$R_{F^2} = 6.6\%$, $R_{F^2w} = 8.0\%$, $R_F = 4.0\%$
Neutron powder data: $Bi_4V_2O_{11}$	$R_B = 4.8\%$, $R_F = 3.7\%$		$R_B = 5.6\%$, $R_F = 5.8\%$
$Bi_4V_2O_{11}$ purity (weight fract. %)	97(1)%		97(1)%

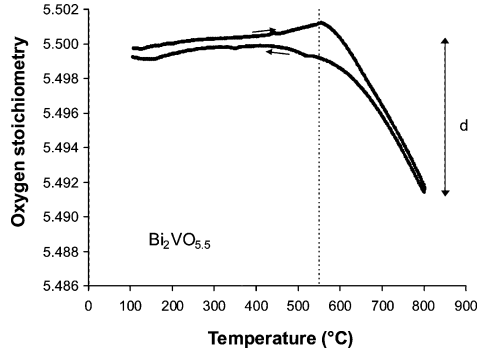

Fig. 1. Variation of the oxygen stoichiometry in $Bi_4V_2O_{11}$ versus temperature (prior to the TGA, the powder was annealed under pure oxygen for 12 h at 800 °C and slowly cooled (20 °C/h) in the same atmosphere).

Moreover, to avoid any risk of partial reduction during data collection of neutron powder thermodiffraction, a vanadium furnace equipped with a silica tube open to air was used.

3.2. Refinement of γ-$Bi_4V_2O_{11}$

The crystal structure of γ-$Bi_4V_2O_{11}$ was refined, starting from the previously published model [11] and using the combined refinement (Fullprof) of X-ray single crystal data and neutron powder data. Convergence of the refinement was easily obtained. The observed, calculated and difference profiles of the neutron Rietveld are shown in Fig. 2. The modulations observed in the background are mainly due to the silica tube with a likely contribution of disordered

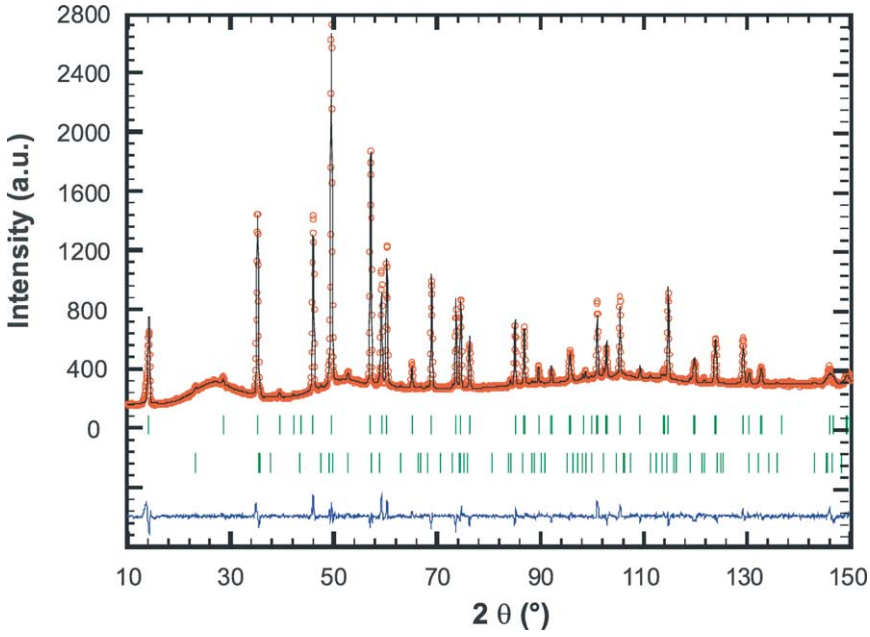

Fig. 2. Neutron Rietveld refinement of γ $Bi_4V_2O_{11}$. The upper curve illustrates the observed and calculated data and the lower is the difference between observed and calculated data. The positions of all allowed Bragg reflections are indicated by vertical tick marks: $Bi_4V_2O_{11}$ (upper) and $BiVO_4$ (lower).

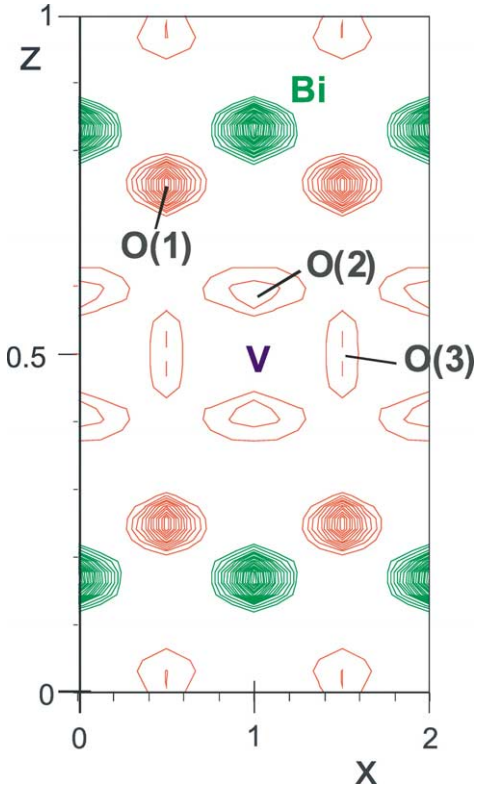

Fig. 3. A typical Fourier map corresponding to the nucleon density at $y = 0$ in γ $Bi_4V_2O_{11}$.

oxygen in the oxide conductor. A typical direct Fourier map corresponding to the nucleon density is shown in Fig. 3. The O(1) atoms of the Bi_2O_2 layers are well defined, while, in contrast, a large spread of the nucleon densities corresponding to the O sites around V is observed. The main difference between the new structural model and the previous one concerns the O sites of the vanadium environment. They were localised in 4e and 8g in the starting model but here the best solution was obtained using 16n sites for both apical O(2) and equatorial O(3) positions.

During the refinement process some constraints were used: the total stoichiometry corresponding to O(2) and O(3) sites was fixed to 7 owing to the global $Bi_4V_2O_{11}$ formula and similar atomic displacement parameters were used for O(2) and O(3). The refined occupancy ratio for O(2) and O(3) are similar. Introduction of anisotropic atomic displacement parameters did not significantly improve the refinement according to the Hamilton criteria and therefore isotropic ones were kept (Table 2).

Using only the neutron powder data, the structure can be refined with bismuth localised only in the idealised 4e site on the four-fold axis. But, on X-ray single crystal data, starting with this Bi on the 4e site, the residual electronic density around this site could not be taken into account even with anisotropic displacement parameters, and to better modelise all this electronic density the Bi atoms were split on: one Bi(1) placed on the idealised 4e site and another one Bi(2) off, on a 16m site, both with partial occupancy. Owing to the strong correlation between these sites, their occupancies were not refined but fixed to ascribe the same weight to each one. Introduction of these two Bi sites significantly improved the conventional R value of the X-ray data (about 3%), and thereby this model was used in the final combined refinement leading to the data reported in Table 3.

A partial view of the γ crystal structure is given in Fig. 4. It is limited to one type of V–O surrounding with its neighbouring Bi–O parts of the Bi_2O_2 Aurivillius-type sheets. A complex relationship is likely to exist between the

Table 2
γ-$Bi_4V_2O_{11}$ structural parameters from combined X-ray single crystal and neutron powder diffraction data

Atom	Site	Occupancy	x	y	z	U_{iso} (Å^2)
Bi(1)	4e	0.5	0	0	0.1740(3)	0.030(1)
Bi(2)	16m	0.125	0.055(2)	0.055(2)	0.1629(4)	0.030(1)
V	8h	0.25	0.030(7)	0.030(7)	1/2	0.048(6)
O(1)	4d	1	0	1/2	1/4	0.047(2)
O(2)	16n	0.238(2)	0	0.134(3)	0.4068(4)	0.094(4)
O(3)	16n	0.198(2)	0	0.431(4)	0.0335(6)	0.094(4)

Table 3
β-$Bi_4V_2O_{11}$ structural parameters from combined X-ray single crystal and neutron powder diffraction data in *Amam* space group

Atom	Pos.	Occ.	x	y	z	U_{11}	U_{22}	U_{33}	U_{12}	U_{13}	U_{23}	U_{eq} (Å^2)
Bi(1)	8e	1	0	0	0.1697(3)	0.042(2)	0.051(2)	0.029(2)	−0.0008(4)	0	0	0.041(2)
Bi(2)	8g	1	1/4	0.5381(3)	0.1684(3)	0.035(2)	0.0285(6)	0.028(2)	−0.009(3)	−0.011(3)	−0.0071(8)	0.031(2)
V(1)	8f	0.5	0.018(3)	0.471(6)	0	0.02(2)	0.05(2)	0.03(2)	0.003(7)	0	0	0.03(2)
V(2)	4c	1	1/4	0.045(3)	0	0.037(8)	0.044(3)	0.018(8)	0	0	0	0.033(7)
O(1)	16h	1	0.1210(9)	0.2517(9)	0.2490(4)	0.026(2)	0.032(2)	0.050(2)	0.008(2)	0.010(3)	−0.005(5)	0.036(2)
O(2)	8g	1	1/4	0.941(2)	0.1015(5)	0.20(2)	0.088(7)	0.027(3)	0	0	0.026(4)	0.105(9)
O(31)	8f	1	0.124(2)	0.225(3)	0	0.133(9)	0.107(8)	0.25(2)	0.078(7)	0	0	0.16(2)
O(32)	16h	0.75	0.075(2)	0.654(3)	0.0631(6)	0.21(2)	0.31(2)	0.125(8)	0.16(2)	−0.094(9)	−0.16(2)	0.22(2)

$U_{eq} = \frac{1}{3}(\sum_i \sum_j U_{ij} a_i^* a_j^* a_i a_j)$ reduced to $U_{eq} = \frac{1}{3}(\sum_i U_{ii})$ in the case of an orthorhombic form.

occupancy of the apical O(2) sites localised off the four-fold axis and the Bi split-sites.

The mean V–O octahedron is encaged between eight Bi sites but too short O–O contacts, due to the O(2) and O(3) split-sites, preclude simultaneous occupation of many of these O sites. In fact, the V–O environment which appears as an octahedron squashed along the c stacking direction, must be viewed as the result of superimposed polyhedra. Indeed, by selecting appropriate O sites among those drawn, the classical O environments of the V^V cation are easily recognised: octahedron (upper left), tetrahedron (upper right), trigonal bipyramid (down left) and tetragonal pyramid (down right), with interatomic distances compatible with O atomic size. The high degree of disorder of this crystal structure is obviously correlated to the high diffusion of the oxide anions in this polymorph: the anionic conductivity σ is about 0.20 $S \cdot cm^{-1}$ at 670 °C [11].

3.3. Determination of the β-$Bi_4V_2O_{11}$ crystal structure

A partial model of this crystal structure had already been proposed [25] from single crystal X-ray diffraction data, but it was incomplete, the O atomic positions of the V–O environment remained undetermined.

For this study, two strategies were used: (i) a combined refinement of X-ray and neutron data starting with the partial model and classical Fourier difference maps (ii) an *ab initio* determination by direct methods using the neutron powder data. By direct methods, the distribution of the normalized structure factors was clearly in agreement with the choice of a centrosymmetric space group. This was coherent with the ferroelectric-paraelectric character of the $\alpha \rightarrow \beta$ phase transition evidenced by the existence of a hysteresis loop at room temperature which disappears above the transition temperature [7]).

We chose the same *Amam* space group as in the previous study, a non-standard setting of *Cmcm* (No. 63), to keep the stacking direction along the c crystallographic unit cell in both γ and β-polymorphs. The O atomic positions of the V–O environment were revealed and finally the same solution was obtained by both methods. The final atomic positions, occupancies and anisotropic displacement parameters are given in Table 3. The observed, calculated and difference profiles of the neutron Rietveld are shown in Fig. 5.

The V–O polyhedra are reported in Fig. 6. They are composed of infinite zig-zag chains extending along the [100] direction. Each link is built up from one V(2) tetrahedron, one V(1) trigonal bipyramid and another V(2) tetrahedron sharing vertices. The different links are perpendicular to each other and oriented along the $[100]\gamma = [010]\gamma$ directions of the tetragonal γ-polymorph. Moreover, the ellipsoids corresponding to the anisotropic atomic displacements of the O atoms are mainly elongated along the same directions.

The V–O environments are detailed in Fig. 7. The V(2) one is a classical tetrahedron with two V–O bond lengths of 1.668(9) and 1.74(2) Å for V(2)–O(2) and V(2)–O(3), respectively (Table 4). The V(1) oxygen environment is more complex and reveals the partial disorder remaining in this polymorph. In fact, two V(1) half occupied positions very close to each other (0.51(5) Å) are generated by the 8f site. For reason of clarity only one position is drawn in Fig. 7. The apparent V(1) environment involves two O(3) and four O(4) but, due to the stoichiometry of the compound, the O(4) position has a 75% occupancy, three about four of the O(4) positions can be statistically occupied. If it is assumed that for instance the $O(4)_1$ site is vacant (in yellow

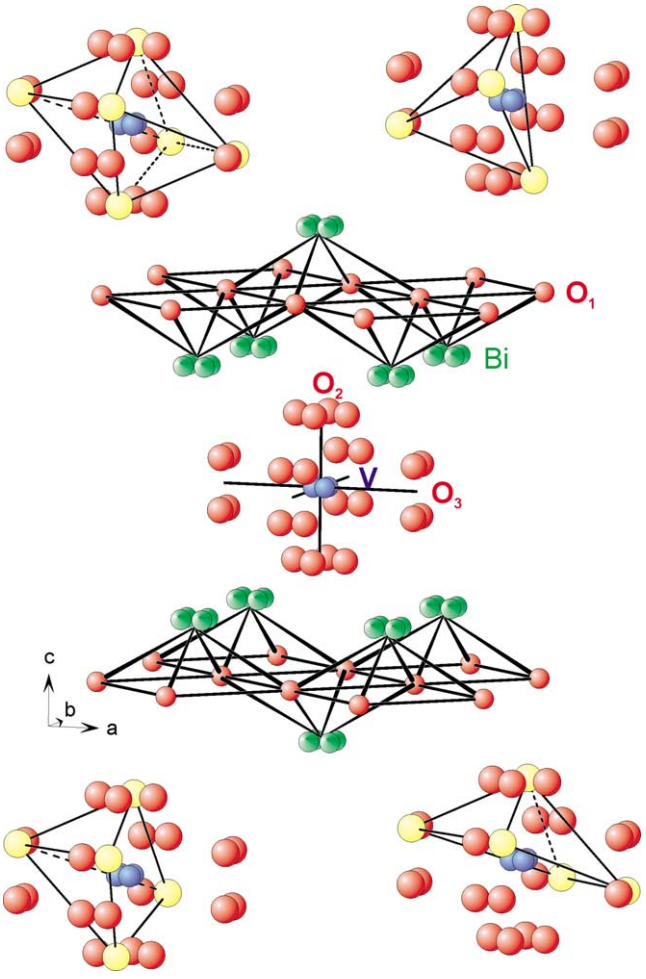

Fig. 4. γ-$Bi_4V_2O_{11}$ crystal structure, limited to one V–O environment with its neighbouring Bi–O parts of the Bi_2O_2 Aurivillius-type sheets. The V–O environment must be viewed as the result of surimposed polyhedra (octahedron, tetrahedron, trigonal bipyramid and tetragonal pyramid).

colour in Fig. 7), the actual V(1) environment is a one side elongated trigonal bipyramid made of three basal O(4) atoms and two apical O(3) atoms. The V–O bond lengths are 1.82(4) and 2.33(4) Å for the apical sites and 1.56(3) Å and 1.59(3) Å for the trigonal basal ones (Table 4). However, this configuration is characterised by a too short interatomic O(4)–O(4) distance of 1.94(2) Å but these oxygen sites display large anisotropic atomic displacement parameters and this apparent unrealistic distance is likely the result of a spread distribution of these oxygen ions. Considering the atom is localised on one extremum along the largest ellipsoid axis, and not at the centre of this ellipsoid, an interatomic distance of 2.5 Å can be calculated (Fig. 7). The shift of this atomic position is the result of the relaxation of the O atoms due to the vacant neighbouring site. As the oxygen vacancy is randomly and statistically distributed over all the four O(4) sites, an average position with large anisotropic displacement is observed by diffraction methods. This behaviour is usually observed in ionic conductor materials.

The atomic positions for the Bi_2O_2 Aurivillius sheets are shown in Fig. 8a. The O(1) atom network is close to that observed in the γ polymorph with a highly symmetric square arrangement. Two independent bismuth sites were evidenced, they reveal a displacive commensurate modulation along the [100] direction, in agreement with the $a_\beta = 2a_m$ superstructure of this form. A similar displacive modulation is obtained with the V positions. In fact, the Bi cations have to accommodate the distortions resulting from the ordering of distinct V–O polyhedra. This coupling generates the modulation depicted on Fig. 8a.

Another feature can be pointed out. It is commonly admitted, for reason of clarity, to describe the crystal structure of the Aurivillius phases using distinct Bi_2O_2

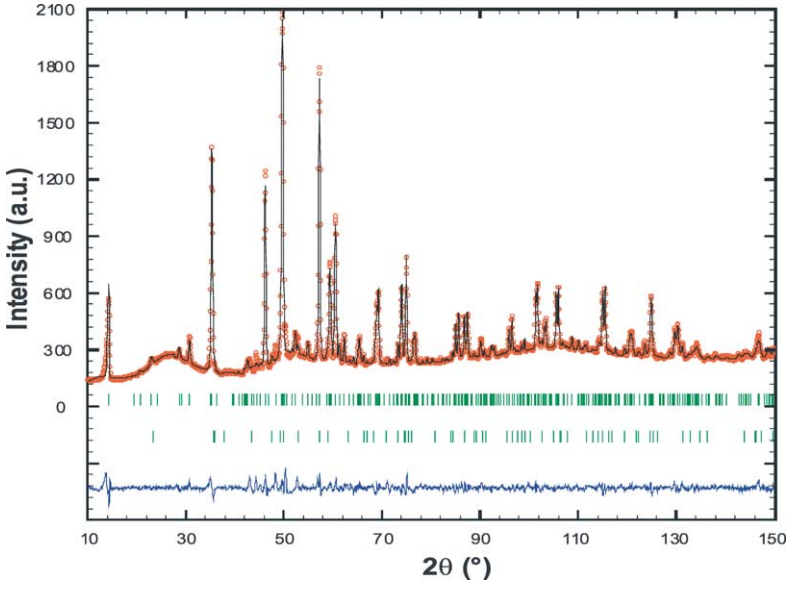

Fig. 5. Neutron Rietveld refinement of β $Bi_4V_2O_{11}$. The upper curve illustrates the observed and calculated data and the lower is the difference between observed and calculated data. The positions of all allowed Bragg reflections are indicated by vertical tick marks: $Bi_4V_2O_{11}$ (upper) and $BiVO_4$ (lower).

sheets on the one hand and perovskite-like slabs on the other hand. This very oversimplified description implicitly assumes that the binding interactions between the slabs can be neglected.

In fact, considering for instance the simple stoichiometric Bi_2WO_6 first member of this family, tight binding calculations performed on this compound clearly indicated that the situation is more complicated: relatively strong bonds are formed between some oxygen atoms of the WO_4^{2-} perovskite-like layer and bismuth. This interaction transfers electron density from the oxygen lone pairs to empty Bi–O σ^* orbitals, and this in turn creates structural deformations within the $Bi_2O_2^{2+}$ layer [35].

A similar situation is likely to occur in the $Bi_2VO_{5.5}\square_{0.5}$ oxygen under stoichiometric compound. The highly disordered crystal structure of the tetragonal γ-form renders speculative any discussion about the Bi–O bond lengths. But the more ordered β-form clearly reveals interactions between Bi atoms and some O atoms of the V–O layers, with 2.68(6) Å and 2.63(6) Å distances for Bi(1)–O(4) and Bi(2)–O(4), respectively (Table 4).

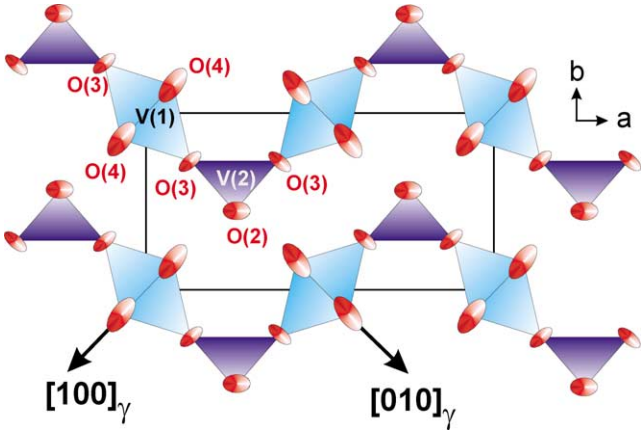

Fig. 6. Projection along [001] of the V–O sheets in β $Bi_4V_2O_{11}$.

A possible scheme for the $\gamma \leftrightarrow \beta$ phase transition is illustrated in Fig. 8 where the Bi and O positions of one Bi_2O_2 layer are represented. As the [001] direction is the same in both β and γ forms, the transformation involves the (001) plane. To deduce the square plane γ basis from the rectangular β one (Fig. 8a), a_β has to be transformed

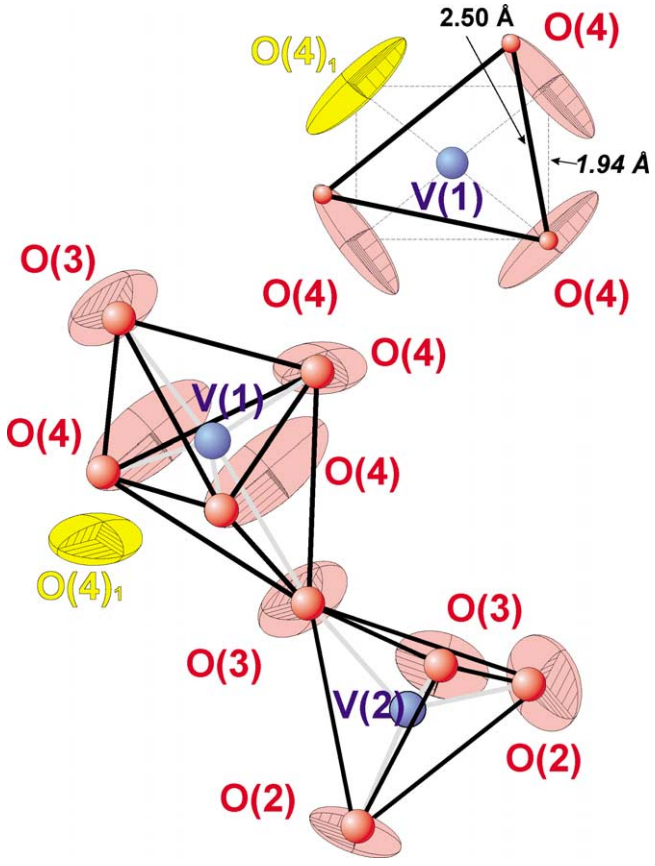

Fig. 7. V–O environments in β $Bi_4V_2O_{11}$. For reason of clarity only one V(1) position is drawn.

Table 4
Selected bond lengths (Å) for β $Bi_4V_2O_{11}$

Bi1–O1[1,11]	2.311(8)	V1–V1[5]	0.51(5)	O2–O3[10]	2.65(2)
Bi1–O1[2,8]	2.316(8)	V1–O3[1]	1.82(4)	O2–O4[1,9]	2.61(2)
Bi1–O4[3,7]	2.68(2)	V1–O3[5]	2.33(4)		
		V1–O4[1]	1.56(3)	O3–O3[9]	2.83(3)
Bi2–O1[1,9]	2.497(8)	V1–O4[5]	1.59(3)	O3–O4[1,6]	2.66(3)
Bi2–O1[4,12]	2.271(8)			O3–O4[5,7]	2.52(3)
Bi2–O2[1]	2.49(1)	V2–O2[3,13]	1.668(9)		
Bi2–O4[1,9]	2.63(2)	V2–O3[1,9]	1.74(2)	O4–O4[6]	1.94(2)
				O4–O4[7]	2.42(2)
O1–O1[2]	2.71(2)				
O1–O1[9]	2.89(2)				
O1–O1[4,8]	2.816(7)				
O1–O2[8]	2.92(1)				
O1–O4[8]	2.99(1)				

[1] x, y, z; [2] $-x, 1/2-y, 1/2-z$; [3] $x, y-1, z$; [4] $x, 1/2+y, 1/2-z$; [5] $-x, 1-y, -z$; [6] $x, y, -z$; [7] $-x, 1-y, z$; [8] $x, y-1/2, 1/2-z$; [9] $1/2-x, y, z$; [10] $x, 1+y, z$; [11] $-x, -y, -z$; [12] $1/2-x, 1/2+y, 1/2-z$; [13] $x, y-1, -z$.

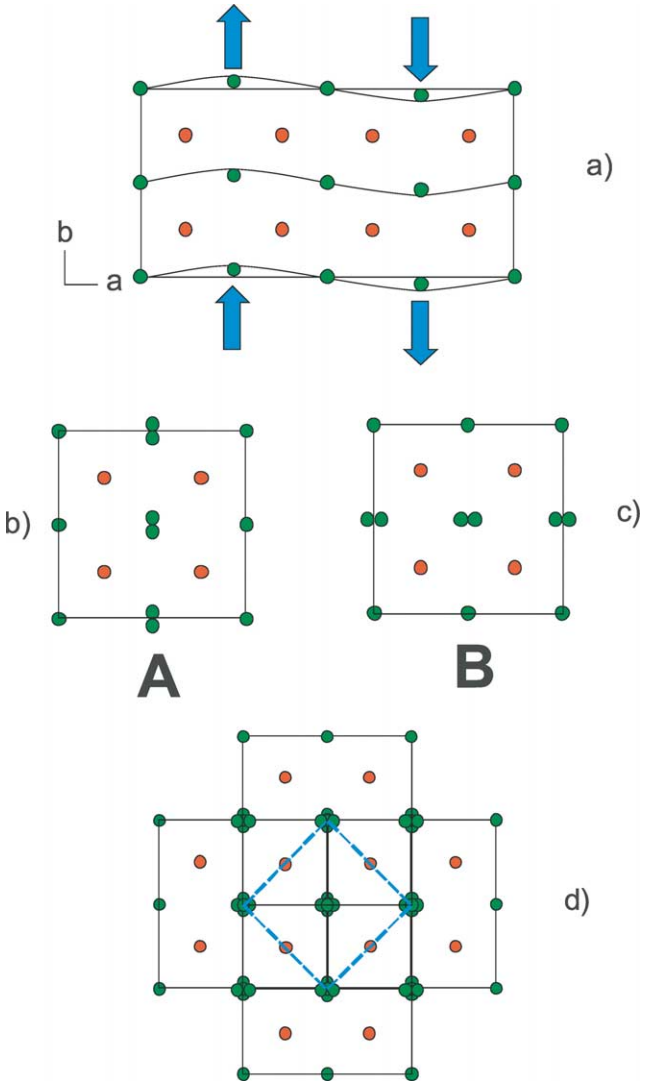

Fig. 8. (a) Bi_2O_2 layers in β $Bi_4V_2O_{11}$, (b)–(d) a possible scheme for the $\gamma \leftrightarrow \beta$ $Bi_4V_2O_{11}$ phase transition.

into $a_\beta/2 = a_m = b_m$, for instance by gliding one half of the rectangular basis over the second one. The configuration of Fig. 8b is obtained (A unit) and another one (Fig. 8c) is obtained by a 90° rotation (B unit). Then combining three A units with three B ones, the scheme of Fig. 6d is deduced, leading to the square plane basis of the γ-unitcell drawn in dotted line. It is worth pointing out that during this transformation the O atomic positions merge and that the Bi split-sites of the γ form are generated: the Bi(1) 4e site on the four-fold axis and the Bi(2) 16m one off the axis, both with equal weight. The Bi(2)–Bi(2) shift calculated in units A and B is equal to 0.43 Å, close to that of 0.44 Å in the γ-form. Starting from the high temperature tetragonal γ-polymorph, the ordering directions along a_m and b_m are potentially equivalent to generate the orthorhombic unitcell of the β-form when decreasing the temperature.

4. Conclusion

Using combined X-ray single crystal and neutron powder thermodiffraction data, the crystal structure of the high temperature γ-form of $Bi_4V_2O_{11}$ was confirmed and accurately refined in the $I4/mmm$ space group, and that of the β-form was entirely determined in the centrosymmetric space group *Amam*. The two-fold supperlattice characterising the β structure is the result of an ordering process involving corner-sharing V–O tetrahedra and disordered trigonal bipyramids.

Acknowledgements

The authors are grateful to Françoise Ratajczak for the powder preparation and to ILL for neutron facilities. Olivier Isnard from the Laboratoire de Cristallographie of Grenoble is acknowledged for his help during the neutron diffraction experiment. The development of BIMEVOX-based COG are the subject of a “Contrat de programme de recherche” (CPR) between L’Air Liquide and the CNRS within the CNRS “Programme Matériaux” framework.

References

[1] A.A. Bush, Yu.N. Venevtsev, Russ. J. Inorg. Chem. 31 (1986) 769.
[2] V.G. Osipyan, L.M. Savchenko, V.L. Elbakyan, P.B. Avakyan, Russ. J. Inorg. Chem. 23 (1987) 467.
[3] V.N. Borisov, V.M. Pashkov, Yu.M. Poplavko, P.B. Avakyan, V.G. Osipyan, Izv. Akad. Nauk SSSR, Ser. Fiz. 54 (1990) 1221.
[4] K.V.R. Prasad, K.B.R. Varma, J. Phys. D: Appl. Phys. 24 (1991) 1858; J. Mater. Sci. 30 (1995) 6345; Mater. Chem. Phys. 38 (1994) 406.
[5] K.V.R. Prasad, A.R. Raju, K.B.R. Varma, J. Mater. Sci. 29 (1994) 2691.
[6] S.K. Ramasesha, A.K. Singh, K.B.R. Varma, Mater. Chem. Phys. 48 (1997) 136.
[7] K. Shantha, K.B.R. Varma, Solid State Ionics 99 (1997) 225; K. Shantha, K.B.R. Varma, J. Mater. Res. 14 (1999) 476; K. Shantha, K.B.R. Varma, Mater. Sci. Eng. B 60 (1999) 66.
[8] M. Joseph, H.Y. Lee, H. Tabata, T. Kawai, J. Appl. Phys. 88 (2000) 1193.
[9] T. Sakai, T. Watanabe, Y. Cho, K. Matsuura, H. Funakubo, Jpn. J. Appl. Phys. (Part 1) 40 (2001) 6481.
[10] F. Abraham, M.-F. Debreuille-Gresse, G. Mairesse, G. Nowogrocki, Solid State Ionics 28–30 (1987) 529.
[11] F. Abraham, J.-C. Boivin, G. Mairesse, G. Nowogrocki, Solid State Ionics 40–41 (1990) 934.
[12] T. Iharada, A. Hammouche, J. Fouletier, M. Kleitz, J.-C. Boivin, G. Mairesse, Solid State Ionics 48 (1991) 257.
[13] V. Sharma, A.K. Shukla, J. Gopalakrishnan, Solid State Ionics 58 (1992) 359.
[14] J.B. Goodenough, A. Manthiram, M. Pranthaman, Y.S. Zhen, Mater. Sci. Eng. B 12 (1992) 357.
[15] C.K. Lee, G.S. Lim, K.S. Low, A.R. West, J. Mater. Chem. 4 (1994) 1441.
[16] O. Joubert, A. Jouanneaux, M. Ganne, R.-N. Vannier, G. Mairesse, Solid State Ionics 73 (1994) 309.
[17] J. Yan, M. Greenblatt, Solid State Ionics 81 (1995) 225.
[18] L. Qiu, Y.L. Yang, A.J. Jacobson, J. Mater. Chem. 7 (1997) 249.
[19] P. Kurek, J.R. Dygas, F. Krok, W. Bogusz, Ionics 3 (1997) 299.
[20] G. Mairesse, C. R. Acad. Sci. Paris (Série IIc) 2 (1999) 651.

[21] A.V. Chadwick, C. Colli, C. Maltese, G. Morisson, I. Abrahams, A.J. Bush, Solid State Ionics 119 (1999) 79.
[22] O. Joubert, A. Jouanneaux, M. Ganne, Mater. Res. Bull. 29 (1994) 175.
[23] M. Huvé, R.-N. Vannier, G. Nowogrocki, G. Mairesse, G. Van Tandeloo, J. Mater. Chem. 6 (1996) 1339.
[24] R.-N. Vannier, G. Mairesse, F. Abraham, G. Nowogrocki, E. Pernot, M. Anne, M. Bacmann, P. Strobel, J. Fouletier, Solid State Ionics 78 (1995) 183.
[25] G. Mairesse, Fast Ion Transport in Solids, NATO ASI Series E 250 (1993) 271.
[26] M. Touboul, J. Lokaj, L. Tessier, V. Kettman, V. Vrabel, Acta Crystallogr. C 48 (1992) 1176.
[27] K. Sooryanarayana, T.N. Guru Row, K.B.R. Varma, Mat. Res. Bull. 32 (1997) 1651.
[28] W. Zhou, D.A. Jefferson, H. He, J. Yuan, D.J. Smith, Phil. Mag. Lett. 75 (1997) 105.
[29] I. Abrahams, A.J. Bush, F. Krok, G.E. Hawkes, K.D. Sales, P. Thorton, W. Bogusz, J. Mater. Chem. 8 (1998) 1213.
[30] C.K. Lee, D.C. Sinclair, A.R. West, Solid State Ionics 62 (1993) 193.
[31] Ya.N. Blinovskov, A.A. Fotiev, Russ. J. Inorg. Chem. 32 (1987) 254.
[32] M. Touboul, C. Vachon, Thermochim. Acta 133 (1988) 61.
[33] A. Altomare, G. Cascarano, C. Giacovazzo, A. Guagliardi, M.C. Burla, G. Polidori, M. Camalli, J. Appl. Cryst. 27 (1994) 435.
[34] J. Rodriguez-Carjaval, FULLPROF Program, Version 0.2, 1998.
[35] S. Seong, K.-A. Yee, T.A. Albright, J. Am. Chem. Soc. 115 (1993) 1981.